

# Efficient excitation of nonlinear phonons via chirped mid-infrared pulses: induced structural phase transitions

A.P. Itin<sup>1,2</sup> and M.I. Katsnelson<sup>1</sup>

<sup>1</sup>*Radboud University, Nijmegen, The Netherlands,*

<sup>2</sup>*Space Research Institute, Moscow, Russia*

Nonlinear phononics play important role in strong laser-solid interactions. We discuss nonlinear dynamical protocols which allow for efficient excitation and control of nonlinear phonons. We consider recent inspiring proposals: inducing ferroelectricity in paraelectric material such as  $\text{KTaO}_3$  and inducing structural deformations in cuprates like  $\text{La}_2\text{CuO}_4$  [A. Subedi et.al, Phys. Rev. B 89,220301 (2014), A.Subedi, Phys. Rev. B 95, 134113 (2017)]. High-frequency phonon modes are driven by mid-infrared pulses, and coupled to lower-frequency modes those indirect excitation causes structural deformations. Such proposals are in line with a series of recent experiments on light-induced phase transitions. We study in a more detail the case of  $\text{KTaO}_3$  without strain, where (at first glance) it was not possible to excite the needed low frequency phonon mode by resonant driving of the higher frequency one. Behaviour of the phonon system is explained using a reduced model of coupled driven nonlinear oscillators. We find a dynamical mechanism which prevents effective excitation at resonance driving, and show that for certain detunings of driving frequency from the exact resonance the system response is, counterintuitively, greatly amplified. In order to induce ferroelectricity in  $\text{KTaO}_3$  without a strain we employ driving with sweeping frequency, realizing so called capture into resonance. The method works for realistic femtosecond pulses. Our approach can be applied to other related systems, e.g. laser driven orthorhombic perovskites like  $\text{ErFeO}_3$ .

Research in ultrafast light-control of materials have attracted a lot of interest recently [1–9]. In particular, light-induced phase transitions using near-visible sources have been implemented: insulator-to-metal transition in manganates [3], low-spin to high-spin transition in metal organic frameworks [4], etc. Intense midinfrared pulses have been used to directly control the dynamical degrees of freedom of the crystal lattice [5–9], inducing insulator-to-metal transitions and melting of orbital and magnetic orders. In many recent suggestions and experiments phonon modes are driven indirectly: infrared radiation drives a high-frequency infrared active phonon mode which then excite the needed modes (not easily accessible by direct drive) by means of nonlinear couplings. Here we suggest, in particular, to add a new useful tool to the arsenal of nonlinear phononics: capture into a resonance. Such phenomenon is encountered in classical and celestial mechanics [10–12] and was employed, e.g. in plasma and accelerator physics [13–17].

We find that in our particular system (perovskite paraelectric  $\text{KTaO}_3$ , being described below) there is a possibility to considerably excite the high-frequency phononic mode even with a usual (fixed frequency) pulse, for certain range of non-resonant driving frequencies. However, for efficient indirect excitation of the lower frequency phonon mode, a protocol based on capture into resonance, which requires a pulse with chirped frequency, is very helpful. We show that such protocol is useful for other systems as well, e.g. for cuprates like  $\text{La}_2\text{CuO}_4$  (LCO). The idea of capture into resonance is based on the fact that in a nonlinear system with near-resonant driving, as amplitude of perturbation grows, frequency of the system deviates from its low-amplitude value, and the system stops to absorb energy efficiently. Driving

with changing frequency at certain conditions enables to sustain resonance relation between drive and the system [18]. Pulses with frequency chirps on picosecond timescale have been generated e.g. in FELIX [19].

In all considered examples below, a phonon mode with (at least) quartic nonlinearity is driven by a laser pulse, creating effective potential for a coupled lower-frequency phonon mode those excitation triggers structural phase transition. Neglecting dissipation for a while, our starting Hamiltonian  $H = \frac{P^2}{2} + \frac{\Omega_0^2 Q^2}{2} + c_4 Q^4 - Q F_0 \sin \Phi(t)$ , where  $\Phi(t)$  is the phase of the driving  $\dot{\Phi}(t) = \Omega(t)$ ,  $\Omega_0$  is linear frequency of the driven phonon mode,  $c_4, c_6..$  are anharmonic coefficients,  $F_0(t)$  is the amplitude of the external field. Introducing symplectic coordinates  $P = \sqrt{2I\Omega_0} \cos \phi$ ,  $Q = \sqrt{\frac{2I}{\Omega_0}} \sin \phi$  we then make a transformation to the resonance phase  $\gamma = \phi - \Phi$  using the time-dependent generating function  $W = J(\phi - \Phi)$ . The new Hamiltonian  $H' = H - J\Omega$  can be averaged over the fast phase, with the result  $\mathcal{H} = \delta\Omega J + \frac{3}{2}c_4 \frac{J^2}{\Omega_0^2} - \frac{1}{2}F_0 \sqrt{2J/\Omega_0} \cos \gamma$ . Introducing now  $x = \sqrt{2J} \sin \gamma$ ,  $y = \sqrt{2J} \cos \gamma$ , we get an effective Hamiltonian  $H = \frac{3}{8} \frac{c_4}{\Omega_0^2} (x^2 + y^2)^2 + \frac{\delta\Omega}{2} (x^2 + y^2) - \frac{F_0}{2\sqrt{\Omega_0}y}$ . Upon rescaling  $H \rightarrow H/\frac{3}{8} \frac{c_4}{\Omega_0^2}$ ,  $t \rightarrow t \frac{3}{8} \frac{c_4}{\Omega_0^2}$  and introduction of  $\lambda = -\frac{\delta\Omega}{2}/\frac{3}{8} \frac{c_4}{\Omega_0^2}$ ,  $\mu = -\frac{F_0}{2\sqrt{\Omega_0}}$  we bring the Hamiltonian to the standard form

$$H = (x^2 + y^2)^2 - \lambda(t)(x^2 + y^2) + \mu(t)y. \quad (1)$$

This Hamiltonian is often encountered in problems of celestial mechanics and plasma physics [12]. Under slow change of frequency and/or amplitude of driving, parameters of (1) are also changing (increasing frequency corresponds to  $\dot{\lambda} > 0$ ). Corresponding phase portraits are

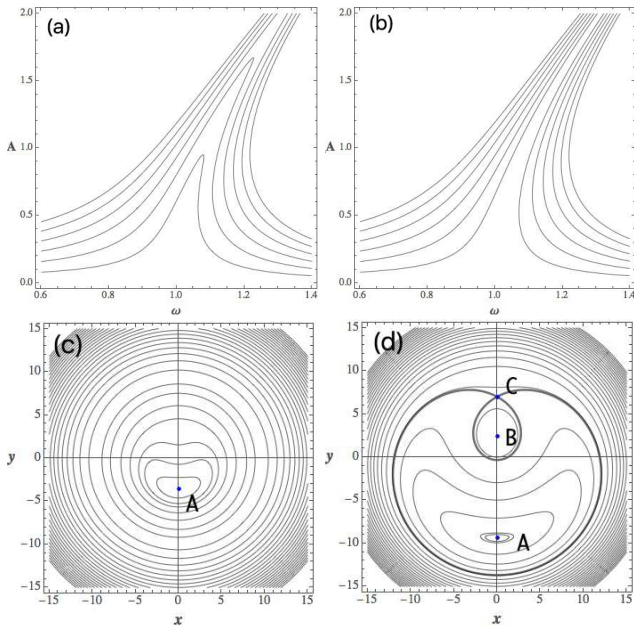


FIG. 1: Top panel: steady states of the driven Duffing oscillator (2) as a function of  $\omega \equiv \Omega/\Omega_0$  at several values of the driving force amplitude  $F_0$  ( $A$  is the amplitude of  $Q$ ). (a) damped Duffing oscillator (b) undamped Duffing oscillator. Curves from bottom to top correspond to:  $E_0 = 5, 10, 15, 20, 25, 30$  MeV cm $^{-1}$ . Bottom panel: phase portraits of the effective Hamiltonian (1) (c).  $\lambda < \lambda_* = \frac{3}{2}\mu^{2/3}$  (d)  $\lambda > \lambda_* = \frac{3}{2}\mu^{2/3}$ .

shown on Fig. (1). A bifurcation happens at  $\lambda_* = \frac{3}{2}\mu^{2/3}$ . Below this value, there is a single equilibrium ( $A$ ), while at higher values of  $\lambda$  there are two stable ( $A, B$ ) and one unstable equilibrium ( $C$ ). Provided certain conditions are met, a phase particle can follow the initial equilibrium point which moves away from origin. This corresponds to growing amplitude of oscillation (capture into the resonance, since staying in the vicinity of the stable point of the effective Hamiltonian means that in the original system the mode oscillates with the frequency being approximately equal to the instantaneous frequency of the drive). In the adiabatic approximation, dynamics can be described in a great detail [12, 18]. E.g., as the parameters of the system are changing, phase space area within the trajectory remains approximate adiabatic invariant, and from behaviour of the areas inside separatrix loops it can be predicted when the phase point will be thrown away from the resonance. In our realistic system nonadiabaticity and dissipation become very important, nevertheless qualitative understanding of dynamics allows to construct simple and effective protocol for phonon excitation. With the dissipation, equation of motion becomes

$$\ddot{Q} + \gamma\dot{Q} + \Omega_0^2 Q + 4c_4 Q^3 = F_0 \sin \Phi(t), \quad (2)$$

which is the same as in a damped and driven Duffing oscillator. At fixed frequency, searching for a periodic solution  $Q = A \sin(\Omega t + \phi_0)$ , one gets a cubic equation

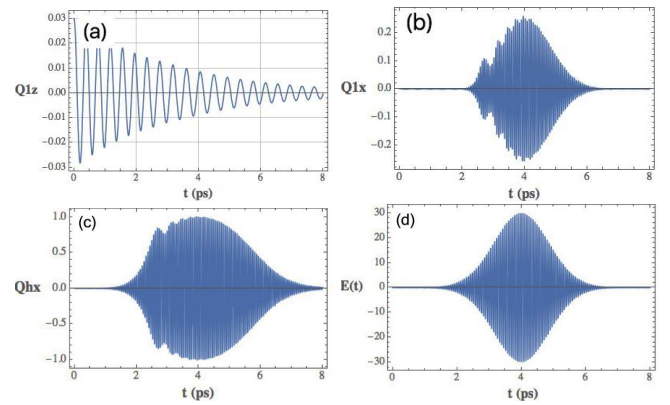


FIG. 2: Dynamics of the system under resonant driving. From top to bottom:  $Q_{1z}, Q_{1x}, Q_{hx}$  modes (in units of  $\dot{A}\sqrt{am\mu}$  [2]), and  $E(t)$  pulse. (in units of MV cm $^{-1}$ ). Time is in picoseconds. Parameters are:  $E_0 = 30$  MV cm $^{-1}$ , damping coefficients  $\gamma_h, \gamma_1$  are 4% of  $\Omega_h, \Omega_1$ , correspondingly. The half-width of the gaussian laser pulse is 2ps. Similar to [2],  $Q_{1z}$  was given a small initial excitation to initiate its dynamics (which may be thought to come from temperature fluctuations). Strong driving of  $Q_{hx}$  and corresponding excitation of  $Q_{1x}$  modes almost do not affect decay of the transverse mode  $Q_{1z}$ , and leaves it unexcited.

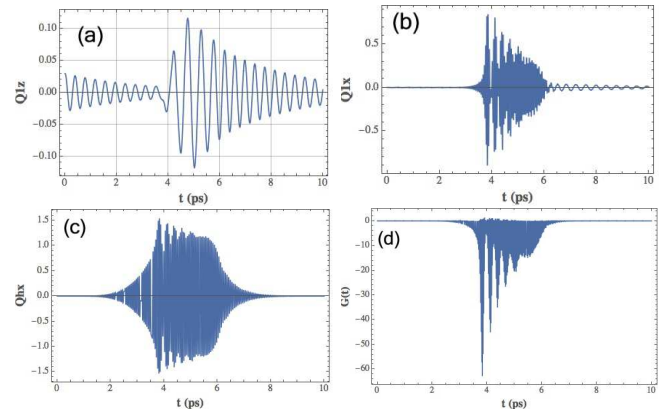


FIG. 3: Dynamics of the system under off-resonant driving with frequency  $\Omega = 1.2\Omega_h$ . From top to bottom:  $Q_{1z}, Q_{1x}, Q_{hx}$  modes, and the instantaneous coefficient  $G(t)$  of the  $(\frac{\Omega^2}{2} + G(t))Q_{1z}^2$  term in the potential energy. The form of the electric field pulse is the same as in Fig.[2] (but with shifted base frequency), and  $Q_{1z}$  mode is now remarkably excited. When  $G(t)$  exceeds  $-\Omega_1^2 \approx -27.06$ , the effective potential for the mode  $Q_{1z}$  becomes unstable. Due to violent beatings in  $Q_{hx}$  mode, it does not happen smoothly, and only a short fraction of the pulse excitation the mode  $Q_{1z}$  experiences the inverted parabolic potential.

for the amplitude of a steady solution:

$$A^2 \left( \gamma^2 \Omega^2 + (\Omega_0^2 - \Omega^2 + 3c_4 A^2)^2 \right) = F_0^2 \quad (3)$$

Solutions of Eq.(3) are shown on Fig. (1a) for different values of the driving amplitude  $F_0$ . They are dissipative counterparts of fixed points in phase portraits of (1) (see

a more detailed discussion in [20]). It is immediately seen that driving with higher than resonant frequency allows to achieve higher steady-state amplitudes. As we will see below, a short laser pulse brings the system far from equilibrium, which is not very good from the point of generating effective potentials for low-frequency modes. Proper phase tailoring of the pulse, especially including chirp of the frequency, allows to achieve drastically better results.

*Induced ferroelectricity.* We start with a specific example of  $\text{KTaO}_3$  for concreteness. As several other  $\text{ABO}_3$  perovskite oxides with cubic structure, it poses a paraelectric phase. These materials have four triply degenerate optical phonon modes at the zone center. Three of these modes are infrared active (have the irreducible representation  $T_{1u}$  [2]). The remaining one is optically inactive (has the irreducible representation  $T_{2u}$  [2]). Ferroelectricity is related to dynamical instability of an infrared-active transverse optic phonon mode: most ferroelectric materials show a characteristic softening of an infrared transverse optic mode as the transition temperature is approached. In [2] it was investigated if a similar softening and instability of the lowest frequency  $T_{1u}$  mode can be achieved by an intense laser-induced excitation of the highest frequency  $T_{1u}$  mode. In the case of cubic structure it was not achieved due to certain dynamical reasons (being discussed below), however with addition of internal stress which modifies the crystal lattice such mechanism worked. Let us here consider in a more detail the cubic structure case (without stress). The calculated in [2] phonon frequencies are  $\Omega_1 = 85 \text{ cm}^{-1}$  and  $\Omega_h = 533 \text{ cm}^{-1}$  for the lowest and highest frequency  $T_{1u}$  modes, respectively ( $\Omega_0$  from previous discussion plays the role of  $\Omega_h$  now). Following [2] we simplify analysis by considering a case where the  $x$  component of the highest frequency mode  $Q_{hx}$  is pumped by an intense light source and influences the dynamics of the lowest frequency  $T_{1u}$  modes along the longitudinal  $Q_{1x}$  and transverse  $Q_{1z}$  coordinates. Dynamics along the second transverse coordinate  $Q_{1y}$  is ignored (assuming that it is qualitatively similar to that of the  $Q_{1z}$  coordinate). The energy surface  $V(Q_{hx}, Q_{1z}, Q_{1x})$  has a complicated form with many kinds of nonlinear couplings and anharmonicities:  $V(Q_{hx}, Q_{1z}, Q_{1x}) + \frac{\Omega_1^2}{2}(Q_{1z}^2 + Q_{1x}^2) + \frac{\Omega_h^2}{2}Q_{hx}^2 + V^{nl}(Q_{hx}, Q_{1z}, Q_{1x})$ , where  $V^{nl}(Q_{hx}, Q_{1z}, Q_{1x})$  is the nonlinear part of the energy, obtained in state-of-the-art calculations of [2], and given in [20] for convenience. Equations of motions are:

$$\begin{aligned} \ddot{Q}_{hx} + \gamma_h \dot{Q}_{hx} + \Omega_{hx}^2 Q_{hx} &= -\frac{\partial V^{nl}(Q_{hx}, Q_{1z}, Q_{1x})}{\partial Q_{hx}} + F(t), \\ \ddot{Q}_{1x} + \gamma_1 \dot{Q}_{1x} + \Omega_1^2 Q_{1x} &= -\frac{\partial V^{nl}(Q_{hx}, Q_{1z}, Q_{1x})}{\partial Q_{1x}}, \\ \ddot{Q}_{1z} + \gamma_1 \dot{Q}_{1z} + \Omega_1^2 Q_{1z} &= -\frac{\partial V^{nl}(Q_{hx}, Q_{1z}, Q_{1x})}{\partial Q_{1z}}. \end{aligned} \quad (4)$$

where  $\gamma_h$  and  $\gamma_1$  are damping coefficients (typically few percents of the corresponding harmonic frequencies), ex-

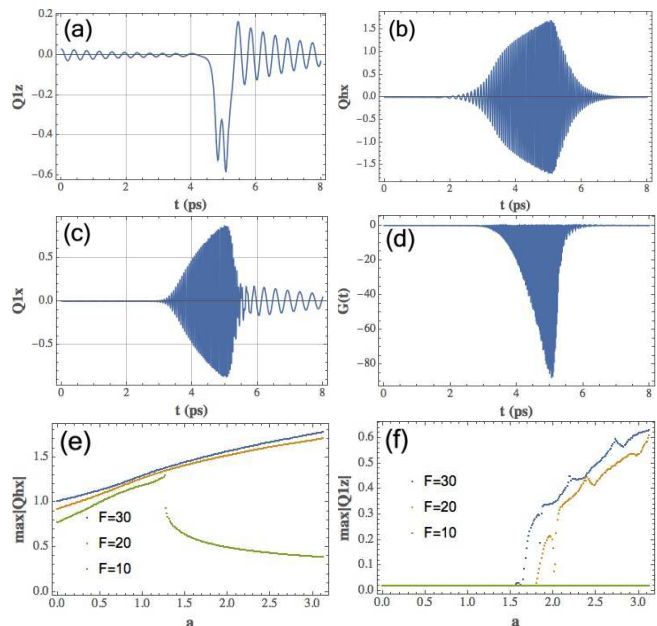


FIG. 4: Dynamics of the  $\text{KTaO}_3$  model system under driving with swept frequency. Instantaneous frequency in the center of the pulse is  $\Omega = 1.2\Omega_h$ . (a-d)  $Q_{1z}$ ,  $Q_{1x}$ ,  $Q_{hx}$  modes, and the instantaneous coefficient  $G(t)$  of the  $(\frac{\Omega_1^2}{2} + G(t))Q_{1z}^2$  term in the potential energy. (e,f) Maximal amplitude of (e)  $Q_{hx}$  and (f)  $Q_{1z}$  modes under driving with sweeping frequency at different sweeping rates  $a$ . Curves from top to bottom correspond to amplitudes of driving  $F_0 = 30, 20, 10 \text{ MV cm}^{-1}$ . Damping rates are 5% of the linear frequencies. Instantaneous frequency of the drive is linearly increased, reaching the linear frequency of the phonon mode  $\Omega_h$  at  $t_* = 0.75\sigma$  before the maximum of the pulse (and increasing afterwards). The pulse width at half-maximum is  $\sigma = 2 \text{ ps}$ . Additional moderate improvement can be achieved by varying  $t_*$  (not shown).  $a = 0$  corresponds to the drive with the constant frequency  $\Omega = \Omega_h$ .

ternal force  $F(t) = Z_{hx}^* E_0 \sin(\Omega t) e^{-t^2/2\sigma^2}$ ,  $Z_{hx}^*$  is the effective charge and  $\Omega$  is the driving frequency.

Qualitative understanding of possible dynamics can be caught by drawing projection of potential energy  $V(Q_{1z}, Q_{1x}, Q_{hx})$  by the plane  $Q_{1x} = 0$  (see Fig. 3 of [2] and [20]). Resulting curves  $V(Q_{1z})|_{Q_{hx}}$  at fixed values of  $Q_{hx}$  has single-well form (at small absolute values of  $Q_{hx}$ ), or a double well form (at larger  $Q_{hx}$ ). In the latter case, induced ferroelectricity is possible, as finite value of  $Q_{1z}$  at equilibrium corresponds to ferroelectric phase. However, to reach such a state dynamically is a non trivial issue. Excitation of  $Q_{hx}$  mode should be done with a pulse of limited power and duration. It is important therefore to understand how to tailor the laser pulse for efficient excitation of the system.

When the driving frequency  $\Omega$  is chosen very close to the  $\Omega_0 \equiv Q_{hx}$  phonon mode frequency  $\Omega_h$  [2], the longitudinal modes  $Q_{hx}$  and  $Q_{1x}$  are both excited, but the transverse mode  $Q_{1z}$  remains almost unaffected. This case is shown on Fig. (2). The reason for this is in-

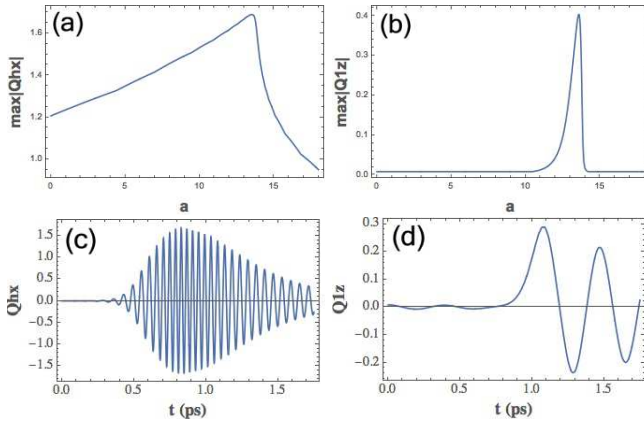


FIG. 5: Excitation by a 350-femtosecond pulse. (a,b) Maximal amplitude of modes  $Q_{hx}$ ,  $Q_{1z}$  under driving with sweeping frequency at different sweeping rates  $a$ . (c) Mode  $Q_{1z}$  at  $a=13.2$  (d) Mode  $Q_{hx}$  at  $a=13.2$ . Damping rates are 5% of the linear frequencies. Instantaneous frequency of the drive is linearly increased, reaching the linear frequency of the phonon mode  $\Omega_h$  at  $t_* = 0.75\sigma$  before the maximum of the pulse (and increasing afterwards). The pulse width at half-maximum is  $\sigma = 0.35$  ps.  $a = 0$  corresponds to the drive with the constant frequency  $\Omega = \Omega_h$ .

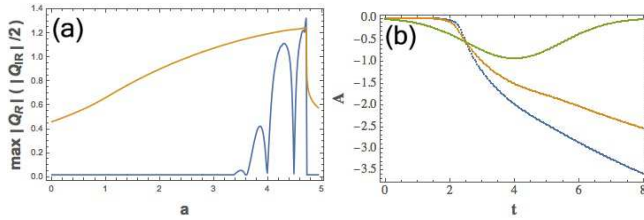


FIG. 6: (a) Maximal amplitude of modes  $Q_{IR}$ ,  $Q_R$  in the driven LCO system under driving with sweeping frequency at different sweeping rates  $a$  (for clarity rescaling is done, and  $Q_{IR}/2$  is shown (top curve) ) (b) corresponding properties of the effective Hamiltonian (Location of the stable equilibrium of effective potential as a function of time for 3 different values of sweeping rates. Only the lowest curve lead to excitation of the Raman mode). ( Damping rates are 5% of the linear frequencies. Instantaneous frequency of the drive is linearly increased, reaching the linear frequency of the phonon mode  $\Omega_h$  at  $t_* = 0.75\sigma$  before the maximum of the pulse (and increasing afterwards).  $\sigma = 2$  ps.

sufficient amplitude of the  $Q_{hx}$  mode. In [2], amplitude of driving was varied in large range, up to pump amplitudes of  $100MVcm^{-1}$ , with no sign of dynamical instability in  $Q_{1z}$ . We show in [20] (see Fig. (S1) ) that increase of pump amplitude makes the dynamics of  $Q_{hx}$ ,  $Q_{1x}$  chaotic, but does not result in any noticeable response of  $Q_{1z}$  mode. This is an interesting dynamical phenomenon: despite very strong driving of  $Q_{hx}$ , dynamical regime with double-well behaviour of mode  $Q_{1z}$  cannot be reached. The reason is that at strong driving the 'auxiliary' longitudinal mode  $Q_{1x}$  becomes excited ([20]), and resulting chaotic dynamics prevents efficient

excitation of  $Q_{hx}$  by the electric pulse. Eqs.[4] define a complicated nonlinear system, where various dynamical regimes may occur, and a route to the needed region in phase space can be found. Firstly, we note that there is range of driving frequencies (away from the exact resonance with  $\Omega_h$ ), where a pulse of the same amplitude can effectively excite all three modes, inducing transient dynamical instability in  $Q_z$ . Indeed, shifting driving frequency about 15-20% from the exact resonance with the high frequency phonon mode leads to considerable excitation of the modes  $Q_{1z}$ ,  $Q_{hx}$  (Fig. (3) ). The mode  $Q_{hx}$  experiences beatings which create transient double-well potential for the  $Q_{1z}$  mode (Fig. (3)d). From the full potential energy of the system, we can single out the term quadratic in  $Q_{1z}$  :  $\left(\frac{\Omega_1^2}{2} + G(t)\right) Q_{1z}^2$ , where  $G(t) = m_2 Q_{hx}^4 + d Q_{hx} Q_{1x} + l Q_{hx}^2 + p Q_{1x}^2 + e_2 Q_{hx}^2 Q_{1x}^2 + e_3 Q_{hx}^3 Q_{hx}$  (see [20] for values of coefficients, for simplicity we keep only the most important ones). We note that due to strong coupling between  $Q_{hx}$  and  $Q_{1x}$  modes, the latter oscillates synchronously with the former, even though its linear frequency considerably differs from that of  $Q_{hx}$ . When the average value of the coefficient  $\langle G(t) \rangle$  exceeds  $-\Omega_1^2/2$ , the effective potential for the mode  $Q_{1z}$  becomes unstable. Due to violent beatings in the  $Q_{hx}$  mode, it does not happen smoothly, and only a short fraction of the pulse excitation time the mode  $Q_{1z}$  experiences the inverted parabolic potential (at the first maxima of the beatings, see Fig. (3)d). There is a way to create the needed effective potential in a more robust way. Consider driving with the sweeping frequency. A chirped pulse have the form  $F = F_0(t) \sin \Phi(t)$ , where  $\Phi(t) = \Omega_0 t + \frac{\alpha t^2}{2}$ ,  $F_0(t) = \exp(-t^2/2(\sigma/2\ln 2)^2)$ . Time-dependence of the instantaneous frequency and the amplitude translates into dependence of parameters  $\mu$ ,  $\lambda$  of the Hamiltonian (1) on time. Corresponding phase portraits are slowly deformed, and, if our phase point is not thrown away from the region where the initial equilibrium is located (see [18, 20] for details), it oscillates around the equilibrium point moving away from the origin. Such regime, illustrated in Fig.(4), not only effective for excitation of the  $Q_{hx}$  mode, but also provides smooth generation of the effective potential for the  $Q_{1z}$  mode (Fig.(4)d). The important feature of the dynamics is that axillary longitudinal mode  $Q_{1x}$  also gets excited considerably. Unlike the case of very strong resonant driving ([20]), where chaotic dynamics happens after excitation of  $Q_{1x}$  mode, here the longitudinal modes oscillate synchronously (in 1:1 resonance), and the resulting dynamics is regular. The strong excitation of the axillary longitudinal mode  $Q_{1x}$  makes the system more complicated: coupled two-mode system can experience chaotic dynamics even in the absence of driving (actually, most of its phase space is chaotic). Regular dynamics happens because the pulse with swept frequency excite the system in such a way that a phase point remains not far from instantaneous equilibrium point. This interesting regime we discuss in [20]. Note that it happens at relatively low damping.

Damping parameters are not known exactly, but typically are 5-10 % of corresponding linear frequencies. If we assume higher damping for low-frequency phonons, then the axillary longitudinal mode  $Q_{1x}$  is not excited considerably, and dynamics can be understood from driven Duffing oscillator model for the  $Q_{hx}$  mode alone (with small corrections from  $Q_{1x}$ ). While in the Hamiltonian model there are three equilibria above the critical frequency detuning, and a phase point captured into resonance can reach large amplitudes of  $Q$  moving near one of them, damping leads to termination of this process at the tip of the resonance 'tongue', where stable and unstable equilibria collide and annihilate. At weak driving amplitudes, the tips lie at a 'backbone' defined as  $A_{tip} = \frac{F_0}{\gamma\Omega_0}$ ,  $\omega_{tip} = 1 + \frac{3c_4F_0^2}{\gamma^2\Omega_0^3}$ . For a rough estimate of the optimal sweep, assume that a pulse starts with the linear resonance frequency  $\Omega_0$ , and reaches the tip of the resonance 'tongue' at its maximum. Then, the estimate for the sweeping rate is  $\alpha = \frac{3c_4F_0^2}{\gamma^2\Omega_0^3}$ . We make numerical experiments with various sweeping rates and amplitudes of driving (see Fig.4e,f), and find a remarkable improvement in efficiency of excitation compared to pulses with constant frequency. Most exciting, the protocol with sweeping frequency works also for much shorter, sub-picosecond pulses. We show in Fig.5 an example with  $\sigma=350$ fs, which is very much related to laser parameters used in A.Cavalleri group.

*Driven LCO.* We note that the same approach applies not only to the ferroelectric system, but to many other systems, e.g. laser driven LCO [1]. There, the relevant reduced model consists of infrared-active  $Q_{IR}$  mode (described by a driven Duffing oscillator) coupled to Raman mode  $Q_R$  by a quadratic-quadratic term.  $Q_R$  ( $B_{1g}(18)$ ) mode describes in-plane rotations of  $\text{CuO}_6$  octahedra, whereas  $Q_{IR}$  mode describes in-plane stretching of Cu-O bond. The energy surface have form

$$V = \Omega_0^2 \frac{Q_{IR}^2}{2} + \Omega_1^2 \frac{Q_R^2}{2} + c_4 Q_{IR}^4 + b_4 Q_R^4 - \frac{g}{2} Q_{IR}^2 Q_R^2$$

Values of the coefficients were derived in elaborate calculations of [1]. There is a single-potential well around the equilibrium value for  $Q_R$  mode at small amplitudes of  $Q_{IR}$ , which becomes double-well potential at larger amplitudes of  $Q_{IR}$  (instantaneous quadratic potential felt by the slow mode is  $\frac{Q_R^2}{2} (\Omega_1^2 - gQ_{IR}^2)$ , which becomes inverted parabolic potential for sufficiently high amplitudes of the driven  $IR$  mode. The critical value of driving force  $F_c$  depends on detuning  $\delta\Omega \equiv \Omega - \Omega_0$  and can be made

smaller than its value on the resonance (being used in [1]). Indeed, to the first approximation, the averaged potential for the slow mode is  $\frac{Q_R^2}{2} (\Omega_1^2 - gQ_{IR,max}^2/2)$  and becomes unstable at critical value of the fast mode amplitude  $Q_{IR,max} = \Omega_1 \sqrt{2/g}$ . This can be achieved at sufficiently smaller driving force amplitudes provided swept frequency pulse is used. We show corresponding results of numerical calculations in Fig.(6). Fig.(6)c shows also instantaneous locations of stable equilibrium of the effective potential as a function of time for different values of sweeping rates. Note that at nonzero sweeping rate the location of the steady resonant amplitude continues to increase even when the pulse amplitude disappears. This is formally correct (equilibrium resonant amplitude mostly depends on driving frequency and only weakly depends on force amplitude at small driving strengths), but due to nonadiabaticity and dissipation this picture stops to be valid at sufficiently small driving strengths.

Excitation of the in-plane rotations associated with the  $Q_R$  mode can be used to modulate superexchange coupling in this cuprate [1]. Recently there has been a lot of interest in effective models arising from periodic driving [22–27], and the suggested method can be useful for this area of research as well. The proposed method can be useful also for related recent proposals and experiments on driven orthorhombic perovskites (like  $\text{ErFeO}_3$ , see [28, 29]), where three-linear phonon coupling is realized: two high-frequency infrared-active modes are coupled to the third, Raman mode.

To conclude, we demonstrate that drastic improvement in efficiency of excitation of nonlinear phonons can be achieved using chirped pulses. In terms of nonlinear dynamics of reduced classical models, capture into the resonance happens and the driven mode is transferred to a higher amplitude state efficiently, which facilitates instability in the coupled low-frequency modes and corresponding phase transitions. The method is especially impressive in cases where a system cannot be excited by bare increase of the power of drive, like in  $\text{KTaO}_3$ . The approach can be useful in many recent proposals on laser-induced phase transitions, including induced ferroelectricity in perovskites, induced structural transitions in LCO cuprates and orthorhombic perovskites.

We are grateful to A.I.Neishtadt and A.Cavalleri for insightful discussions. The work was supported by NWO via Spinoza prize and by European Research Council (ERC) Advanced Grant No. 338957 FEMTO/NANO.

---

[1] A. Subedi, A. Cavalleri, and A. Georges, Phys. Rev. B 89, R220301 (2014).  
 [2] A. Subedi, Phys. Rev. B 95, 134113 (2017).  
 [3] K. Miyano, T. Tanaka, Y. Tomioka, and Y. Tokura, Phys. Rev. Lett. 78, 4257 (1997).

[4] S. Decurtins, P. Gutlich, C. P. Kohler, H. Spiering, and A. Hauser, Chem. Phys. Lett. 105, 1 (1984).  
 [5] M. Rini, R. Tobey, N. Dean, J. Itatani, Y. Tomioka, Y. Tokura, R. W. Schoenlein, and A. Cavalleri, Nature 449, 72 (2007).

- [6] R. I. Tobey, D. Prabhakaran, A. T. Boothroyd, and A. Cavalleri, *Phys. Rev. Lett.* 101, 197404 (2008).
- [7] M. Först et al., *Phys. Rev. B* 84, 241104(R) (2011).
- [8] A. D. Caviglia, et al., *Phys. Rev. Lett.* 108, 136801 (2012).
- [9] M. Först, et al. *Nat. Mater.* 14, 883 (2015).
- [10] A.T. Sinclair, *Monthly Not. Roy. Astron. Soc.* 160, 169 (1972)
- [11] R.J. Greenberg, *Evolution of Satellite Resonances by Tidal Dissipation*, *Astron. J.* 78, 338 (1973)
- [12] V.I. Arnold, V. V. Kozlov, and A.I. Neishtadt, *Mathematical Aspects of Classical and Celestial Mechanics* (3rd ed., Berlin: Springer, 2006).
- [13] V.I. Veksler, *Dokl. Akad. Nauk SSSR* 43, 346 (1944) [*J. Phys. USSR* 9, 153 (1945)].
- [14] E. M. McMillan, *Phys. Rev.* 68, 143 (1945).
- [15] A.I. Neishtadt and A.V. Timofeev, *ZhETF* 93, 1706 (1987) [*JETP* 66, 973 (1987)].
- [16] A.P.Itin, A.I.Neishtadt, A.A.Vasiliev, *Phys. D* 141, 281(2000).
- [17] A.P.Itin, *Plasma Phys. Rep.* 28, 592 (2002).
- [18] A. I. Neishtadt, A. A. Vasiliev, A. V. Artemyev, *Regular and Chaotic Dynamics* 18, 686 (2013); arXiv::1309.6501 (2013).
- [19] G.M.H. Knippels, A.F.G. van der Meer, R.F.X.A.M. Mols, D. Oepts, P.W. van Amersfoort, *Nucl. Inst. Phys. A.* 375, 150 (1996).
- [20] See Supplementary Information for details of calculations, additional figures, and tables with coefficients.
- [21] M. Hase, M. Kitajima, S. Nakashima, and K. Mizoguchi, *Phys. Rev. Lett.* 88. 067401 (2002).
- [22] N.Goldman, J.Dalibard, *Phys. Rev. X* 4, 031027 (2014).
- [23] J. H. Mentink, K. Balzer, and M. Eckstein, *Nature Comm.* 6, 6708 (2015).
- [24] F.Abdullaev et.al, *Phys. Rev. Lett.* 105, 113901 (2010).
- [25] M. Bukov, M. Kolodrubetz, A. Polkovnikov, *Phys. Rev. Lett.* 116, 125301 (2016).
- [26] A.Eckardt, *Rev. Mod. Phys.* 89, 011004 (2017).
- [27] A.P. Itin, M.I. Katsnelson, *Phys. Rev. Lett.* 115, 075301 (2015).
- [28] D.M. Juraschek, M. Fechner, and N.A. Spaldin, *Phys. Rev. Lett.* 118, 054101 (2017).
- [29] T. F. Nova et.al., *Nat. Phys.* 13, 132 (2017)
-

# Supplemental Materials: Efficient excitation of nonlinear phonons via chirped mid-infrared pulses: induced structural phase transitions

## A. Nonlinear part of the potential energy surface for $\text{KTaO}_3$

The nonlinear part of the potential energy surface is:

$$\begin{aligned}
 V^{nl}(Q_{hx}, Q_{1z}, Q_{1x}) = & \quad (S1) \\
 = & \sum_{k=2}^6 \left( a_{2k}(Q_{1z}^{2k} + Q_{1x}^{2k}) + c_{2k}Q_{hx}^{2k} \right) \\
 & + lQ_{1z}^2 Q_{hx}^2 + m_1 Q_{1z}^4 Q_{hx}^2 + m_2 Q_{1z}^2 Q_{hx}^4 \\
 & + n_1 Q_{1z}^4 Q_{hx}^4 + n_2 Q_{1z}^6 Q_{hx}^2 + n_3 Q_{1z}^2 Q_{hx}^6 \\
 & + t_1 Q_{1x}^3 Q_{hx} + t_2 Q_{1x}^2 Q_{hx}^2 + t_3 Q_{1x} Q_{hx}^3 \\
 & + pQ_{1z}^2 Q_{1x}^2 + q_1 Q_{1z}^4 Q_{1x}^2 + q_2 Q_{1z}^2 Q_{1x}^4 \\
 & + r_1 Q_{1z}^4 Q_{1x}^4 + r_2 Q_{1z}^6 Q_{1x}^2 + r_3 Q_{1z}^2 Q_{1x}^6 \\
 & + dQ_{1z}^2 Q_{1x} Q_{hx} + gQ_{1z}^4 Q_{1x} Q_{hx} \\
 & + \sum_{k=1}^3 e_k Q_{1z}^2 Q_{1x}^{4-k} Q_{hx}^k + \sum_{k=1}^5 u_k Q_{1x}^{6-k} Q_{hx}^k \\
 & + \sum_{k=1}^5 f_k Q_{1z}^2 Q_{1x}^{6-k} Q_{hx}^k + \sum_{k=1}^3 h_k Q_{1z}^4 Q_{1x}^{4-k} Q_{hx}^k
 \end{aligned}$$

Values of the main coefficients are:

TABLE I: The values of the coefficients of the polynomial for energy surfaces of Raman and IR modes obtained in [S1], [S2]. The units of a  $Q^m Q^p Q^n$  term are  $\text{meV } A^{-(m+p+n)}$

Coefficient	Term	$\text{KTaO}_3$	Coefficient	Term	LCO
$\Omega_h^2$	$Q_{hx}^2$	1043.77	$\Omega_0^2$	$Q_{IR}^2$	1462.3
$\Omega_{1z}^2$	$Q_{1z}^2$	27.06	$\Omega_1^2$	$Q_R^2$	103.55
$\Omega_{1x}^2$	$Q_{1x}^2$	27.06	$g$	$-Q_R^2 Q_{IR}^2 / 2$	46.98
$a_4$	$Q_{1z}^4$	47.55	$a_4$	$Q_R^4$	8.36
$c_4$	$Q_{hx}^4$	63.17	$c_4$	$Q_{IR}^4$	103.5

## B. Strong resonant driving: chaotic dynamics

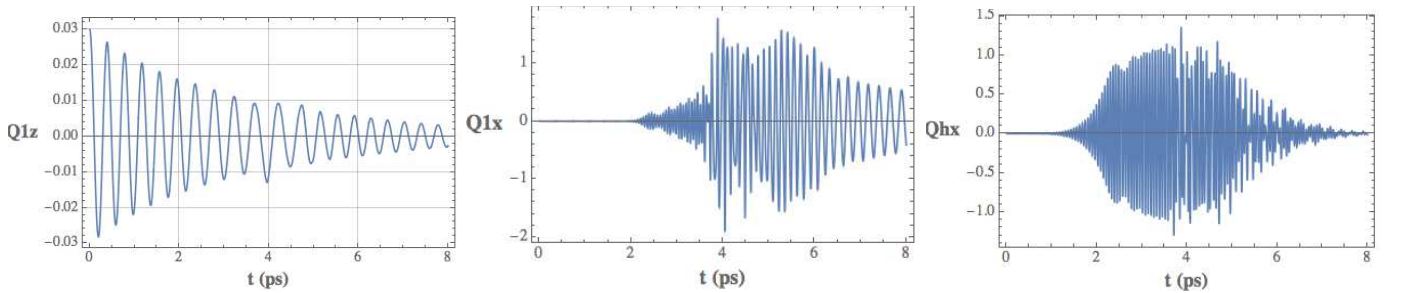


FIG. S1: Resonant driving, the same as in Fig.[2], but with a larger driving amplitude. From left to right:  $Q_{1z}, Q_{1x}, Q_{hx}$  modes, and  $E(t)$  pulse.  $E_0 = 60 \text{ MV cm}^{-1}$ . Amplitude of driving is so large that dynamics become chaotic, nevertheless the mode  $Q_{1z}$  is unexcited.

### C. Two coupled modes with periodic driving

Although the linear frequency of the  $Q_{1x}$  mode is much smaller than that of  $Q_{hx}$ , strong coupling between them causes these modes to oscillate synchronously. One can therefore introduce an effective system combining these modes together and averaging over the driving frequency. The third mode,  $Q_{1z}$  can be neglected until it become excited due to creation of the effective double-well potential. Consider firstly a conservative system, without dissipation.

The reduced two-mode Hamiltonian is (we denote  $Q_1 \equiv Q_{1x}, Q_h \equiv Q_{hx}$ )

$$\begin{aligned} H = & \frac{P_1^2}{2} + \frac{P_h^2}{2} + \Omega_1^2 \frac{Q_1^2}{2} + \Omega_h^2 \frac{Q_h^2}{2} + a_4 Q_1^4 + c_4 Q_h^4 + \\ & + t_1 Q_1^3 Q_h + t_2 Q_1^2 Q_h^2 + t_3 Q_1 Q_h^3 + \sum_{k=1}^5 u_k Q_1^{6-k} Q_h^k + \\ & - Q_h F_0 \sin \Omega t \end{aligned} \quad (S2)$$

Moreover, we neglect the  $u$ -terms in the analytical considerations below, as values of  $t$ -coefficients are considerably higher.

Introducing radial coordinates ( $I_h, \phi_h, I_1, \phi_1$ )

$$\begin{aligned} Q_{hx} &= \sqrt{\frac{2I_h}{\Omega_h}} \sin \phi_h, & P_h &= \sqrt{2I_h \Omega_h} \cos \phi_h, \\ Q_{1x} &= \sqrt{\frac{2I_1}{\Omega_1}} \sin \phi_1, & P_1 &= \sqrt{2I_1 \Omega_1} \cos \phi_1, \end{aligned} \quad (S3)$$

we then switch to rotating phases  $\gamma_h - \Omega t, \gamma_1 - \Omega t$  by means of a generating function

$$W = \rho_h(\phi_h - \Phi) + \rho_1(\phi_1 - \Phi), \Phi \equiv \Omega t \quad (S4)$$

Averaging the resulting Hamiltonian over the explicit time dependence, we get as an effective reduced two-mode Hamiltonian

$$\begin{aligned} H = & \rho_h(\Omega_h - \Omega) + \rho_1(\Omega_1 - \Omega) + \frac{3}{2} c_4 \frac{\rho_h^2}{\Omega_h^2} + \frac{3}{2} a_4 \frac{\rho_1^2}{\Omega_1^2} \\ & + \frac{F_0}{2} \sqrt{\frac{2\rho_h}{\Omega_h}} \sin \gamma_h + \frac{3}{2} t_1 \left(\frac{\rho_1}{\Omega_1}\right)^{3/2} \left(\frac{\rho_h}{\Omega_h}\right)^{1/2} \cos(\gamma_1 - \gamma_h) \\ & + \frac{3}{2} t_3 \left(\frac{\rho_1}{\Omega_1}\right)^{1/2} \left(\frac{\rho_h}{\Omega_h}\right)^{3/2} \cos(\gamma_1 - \gamma_h) \\ & + \frac{1}{2} t_2 \left(\frac{\rho_1}{\Omega_1}\right) \left(\frac{\rho_h}{\Omega_h}\right) (2 + \cos 2(\gamma_1 - \gamma_h)) + \text{u-terms} + \dots \end{aligned} \quad (S5)$$

We then return to cartesian coordinates via  $x_k = \sqrt{\frac{2\rho_k}{\Omega_k}} \cos \phi_k, y_k = \sqrt{2\rho_k \Omega_k} \sin \phi_k$ , and search for equilibria of the resulted two-mode system.

We get two coupled algebraic equations for coordinates of the equilibrium:

$$\begin{aligned} \frac{3}{2} c_4 X_h^3 + X_h \left( \Omega_h^2 (1-x) + \frac{3}{4} t_2 X_1^2 \right) + \frac{9}{8} t_3 X_1 X_h^2 \\ - \frac{3}{8} t_1 X_1^2 &= \frac{F_0}{2}, \\ X_1 \left( \Omega_1^2 (1-x \frac{\Omega_h}{\Omega_1}) + \frac{3}{4} t_2 X_h^2 \right) + \frac{9}{8} t_1 X_1^2 X_h \\ + \frac{3}{2} a_4 X_1^3 - \frac{3}{8} t_3 X_h^3 &= 0 \end{aligned} \quad (S6)$$

$$(S7)$$

If we completely neglect dynamics of  $Q_{1x}$  mode by setting  $X_1 = 0$ , we get a similar picture of the amplitude of excitation of the driven mode as a function of frequency, shown on Fig. S2. There is a qualitative difference with Fig.

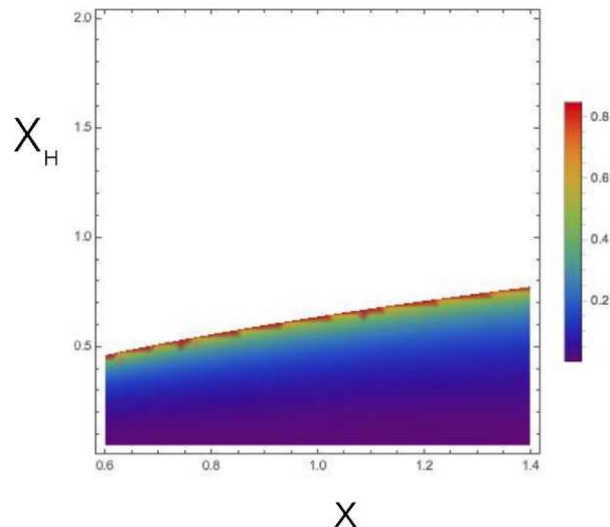


FIG. S2: Steady states of the mode  $X_h$  of the driven reduced two-mode system (S6) without dissipation as a function of frequency  $x \equiv \Omega/\Omega_{hx}$  at several values of the driving force amplitude  $E_0$ . From bottom to top:  $E_0 = 5, 10, 15, 20, 25, 30$  MeV  $\text{cm}^{-1}$ . (b) Steady values of amplitude of the mode  $Q_{1x}$  (i.e.,  $X_1$ ) as a function of  $X_h, x$ . White areas correspond to highest values of  $X_1$

1 in that the resonance 'tongues' are now extended to infinity (as a function of detuning), instead of being rounded up at finite detuning due to damping. This is not so important for a discussion of dynamics below, where we concentrate on instability in  $Q_{1x}$  mode.

Excitation of the second mode ( $Q_{1x}$ ) would deform the picture shown on Fig. S2. More importantly, as amplitude of  $X_h$  grows beyond certain critical value, deviation of  $X_1$  from 0 becomes considerable. Then, dynamics of the system becomes complicated and the first mode stops to absorb the energy from the drive. Note that the steady state value of  $X_h$  in Eq. S6 is a function of  $F_0$  and depends on  $X_1$ , while  $X_1$  is determined from the second equation which does not depend on  $F_0$ . So we could depict a value of  $X_1$  as a density plot on the plane  $(\Omega, X_h)$ : see Fig. S2b. It is clearly seen that as one tries to increase steady amplitude  $X_h$ , above certain curve on  $(\Omega, X_h)$  plane the mode  $Q_{1x}$  becomes excited. Importantly, detuning from the exact resonance to higher frequencies allows to reach higher values of  $X_h$  without considerable excitation of the  $Q_{1x}$  mode. This important qualitative result remains valid in the full system. When we take into account dissipation and the remaining nonlinear coupling terms, the critical curve goes higher, and it becomes possible to reach sufficiently high values of  $X_h$  (again, shifting from the exact resonant to the higher frequencies allows higher values of  $X_h$ ).

---

[S1] A. Subedi, A. Cavalleri, and A. Georges, Phys. Rev. B 89, R220301 (2014).

[S2] Alaska Subedi, arXiv:1612.04788.